



Cite this article: Oprisan SA, Buhusi CV. 2014
What is all the noise about in interval timing?
Phil. Trans. R. Soc. B **369**: 20120459.
<http://dx.doi.org/10.1098/rstb.2012.0459>

One contribution of 14 to a Theme Issue
'Timing in neurobiological processes: from
genes to behaviour'.

Subject Areas:

neuroscience, theoretical biology,
computational biology

Keywords:

striatal beat frequency, interval timing, noise

Author for correspondence:

Sorinel A. Oprisan
e-mail: oprisans@cofc.edu

Electronic supplementary material is available
at <http://dx.doi.org/10.1098/rstb.2012.0459> or
via <http://rstb.royalsocietypublishing.org>.

What is all the noise about in interval timing?

Sorinel A. Oprisan¹ and Catalin V. Buhusi²

¹Department of Physics and Astronomy, College of Charleston, 66 George Street, Charleston, SC 29624, USA
²Department of Psychology, Utah State University, 2810 Old Main Hill, Logan, UT 84332-2810, USA

Cognitive processes such as decision-making, rate calculation and planning require an accurate estimation of durations in the supra-second range—interval timing. In addition to being accurate, interval timing is scale invariant: the time-estimation errors are proportional to the estimated duration. The origin and mechanisms of this fundamental property are unknown. We discuss the computational properties of a circuit consisting of a large number of (input) neural oscillators projecting on a small number of (output) coincidence detector neurons, which allows time to be coded by the pattern of coincidental activation of its inputs. We showed analytically and checked numerically that time-scale invariance emerges from the neural noise. In particular, we found that errors or noise during storing or retrieving information regarding the memorized criterion time produce symmetric, Gaussian-like output whose width increases linearly with the criterion time. In contrast, frequency variability produces an asymmetric, long-tailed Gaussian-like output, that also obeys scale invariant property. In this architecture, time-scale invariance depends neither on the details of the input population, nor on the distribution probability of noise.

1. Introduction

The perception and use of durations in the seconds-to-hours range (interval timing) is essential for survival and adaptation, and is critical for fundamental cognitive processes such as decision-making, rate calculation and planning of action [1]. The classic interval timing paradigm is the fixed-interval (FI) procedure in which a subject's behaviour is reinforced for the first response (e.g. lever press) made after a pre-programmed interval has elapsed since the previous reinforcement. Subjects trained on the FI procedure typically start responding after a fixed proportion of the interval has elapsed despite the absence of any external time cues. A widely used discrete-trial variant of FI procedure is the peak-interval (PI) procedure [2,3]. In the PI procedure, a stimulus such as a tone or light is turned on to signal the beginning of the to-be-timed interval and in a proportion of trials the subject's first response after the criterion time is reinforced. In the remainder of the trials, known as probe trials, no reinforcement is given, and the stimulus remains on for about three times the criterion time. The mean response rate over a very large number of trials has a Gaussian shape whose peak measures the accuracy of criterion time estimation and the spread of the timing function measures its precision. In the vast majority of species, protocols and manipulations to date, interval timing is both *accurate* and *time-scale invariant*, i.e. time-estimation errors increase linearly with the estimated duration [4–7] (figure 1). Accurate and time-scale invariant interval timing was observed in many species [1,4] from invertebrates to fish, birds and mammals such as rats [8] (figure 1*a*), mice [11] and humans [9] (figure 1*b*). Time-scale invariance is stable over behavioural (figure 1*b*), lesion [12], pharmacological [13,14] (figure 1*c*) and neurophysiological manipulations [10] (figure 1*d*).

One of the most influential interval timing paradigms assumes a pacemaker–accumulator clock (pacemaker-counter) and was introduced by

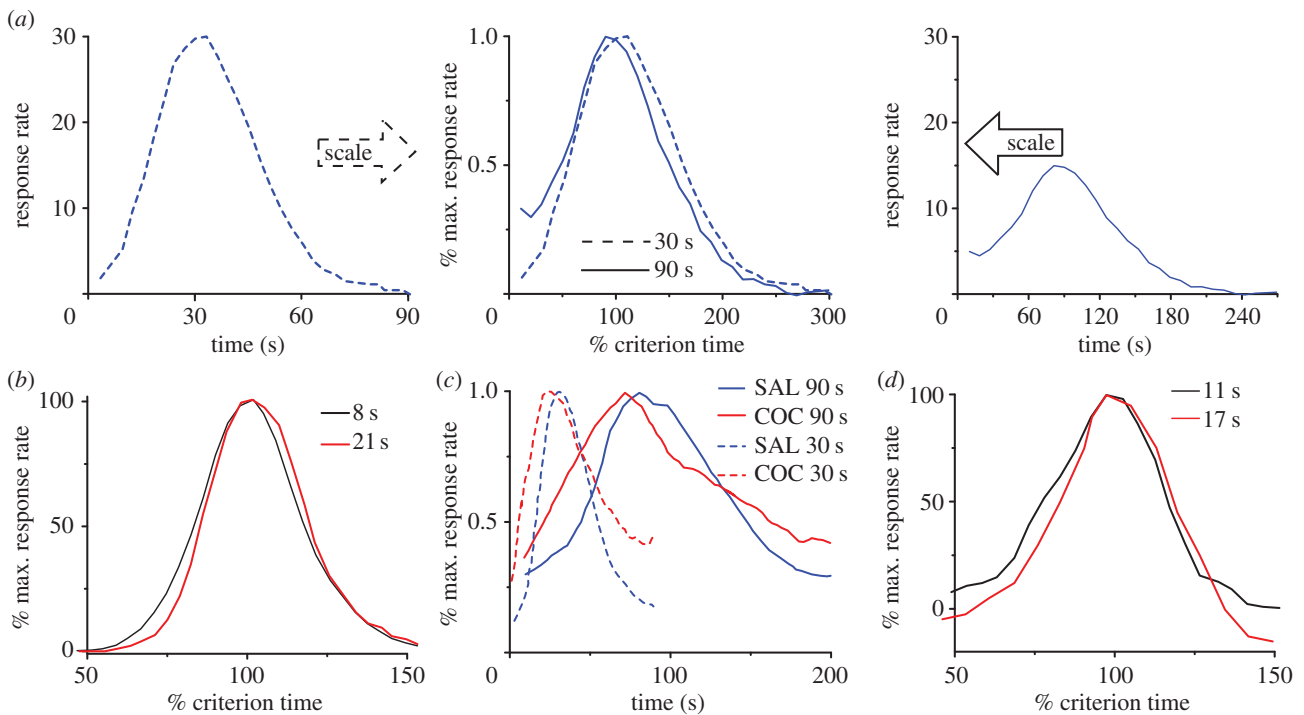


Figure 1. Accurate and time-scale invariant interval timing. (a) The response rate of rats timing a 30 s (left) or 90 s interval (right) overlap (centre) when the vertical axis is normalized by the maximum response rate and the horizontal axis by the corresponding criterion time; redrawn from [8]. (b) Time-scale invariance in human subjects for 8 and 21 s criteria; redrawn from [9]. (c) Systemic cocaine (COC) administration speeds-up timing proportional (scalar) to the original criteria, 30 and 90 s; redrawn from [8]. (d) The hemodynamic response associated with a subject's active time reproduction scales with the timed criterion, 11 versus 17 s; redrawn from [10]. An important feature of the output function is its asymmetry, which is clearly visible in (c). Although all output functions have a Gaussian-like shape they also present a long tail. (Online version in colour.)

Treisman [15]. According to Treisman [15], the interval timing mechanism that links internal clock to external behaviour also requires some kind of store of reference times and some comparison mechanism for time judgement. The model was rediscovered two decades later and became the scalar expectancy theory (SET) [5,16]. SET also assumes that interval timing emerges from the interaction of three abstract blocks: clock, accumulator (working or short-term memory) and comparator. The clock stage is a Poisson process whose pulses are accumulated in the working memory until the occurrence of an important event, such as reinforcement. At the time of the reinforcement, the number of clock pulses accumulated is transferred from the working (short-term) memory and stored in a reference (or long-term) memory. According to the SET, a response is produced by computing the ratio between the value stored in the reference memory and the current accumulator total. To account for the scalar property of interval timing, i.e. the variability of responses is roughly proportional to the peak time, Gibbon [17] showed that a Poisson distribution for the accumulator requires a time-dependent variance in the 'decision and memory factors as well as in the internal clock. These additional sources will be seen to dominate overall variance in performance' (p. 191), emphasizing the important role of cognitive systems in time judgements. For such reasons, SET was considered more a general theory of animal cognition than strictly a theory of animal timing behaviour [18].

Another influential interval timing model is the behavioural timing (BeT) theory [19,20]. BeT assumes a 'clock' consisting of a fixed sequence of states with the transition from one state to the next driven by a Poisson pacemaker. Each state is associated with different classes of behaviour, and the theory claims these behaviours serve as discriminative

stimuli that set the occasion for appropriate operant responses (although there is not a one-to-one correspondence between a state and a class of behaviours). The added assumption that pacemaker rate varies directly with reinforcement rate allows the model to handle some experimental results not covered by SET, although it has failed some specific tests (see [21] for a review).

A handful of neurobiologically inspired models explain *accurate* timing and *time-scale invariance* as a property of the information flow in the neural circuits [22,23]. Buonomano & Merzenich [24] implemented a neural network model with randomly connected circuits representing cortical layers 4 and 3 in order to mimic the temporal-discrimination task in the tens to hundreds of milliseconds range. Durstewitz hypothesized that the climbing rate of activity observed experimentally, e.g. from thalamic neurons recordings [25], may be involved in timing tasks [26]. Durstewitz [26] used a single-cell computational model with a calcium-mediated feedback loop that self-organizes into a biophysical configuration which generates climbing activity. Leon & Shadlen [27] suggested that the scalar timing of subsecond intervals may also be addressed at the level of single neurons, though how such a mechanism accounts for timing of supra-second durations is unclear. A solution to this problem was offered by Killeen & Taylor [28] who explained timing in terms of information transfer between noisy counters, although the biological mechanisms were not addressed.

Population clock models of timing are based on the repeatable patterns of activity of a large neural network that allow identification of elapsed time based on a 'snapshot' of neural activity [29,30]. In all population clock models, timing is an emergent property of the network in the sense that it relies on the interaction between neurons to produce accurate

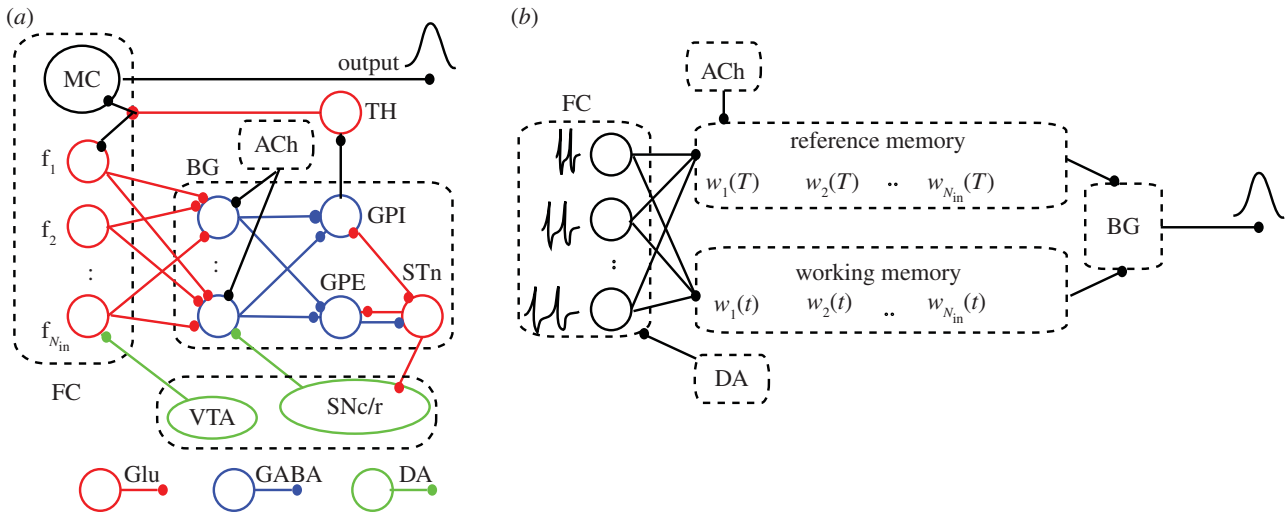


Figure 2. The neurobiological structures involved in interval timing and the corresponding simplified SBF architecture. (a) Schematic of some neurobiological structures involved in interval timing. The colour-coded connectivities among different areas emphasize appropriate neuromodulatory pathways. The two main areas involved in interval timing are frontal cortex and basal ganglia. (b) In our implementation of the SBF model, the states of the N_{in} cortical oscillators (input neurons) at reinforcement time T are stored in the reference memory as a set of weights w_i . During test trials, the working memory stores the state of FC oscillators $v_i(t)$ and, together with the reference memory, projects its content onto N_{out} spiny (output) neurons of the BG. FC, frontal cortex; MC, motor cortex; BG, basal ganglia; TH, thalamus. GPE, globus pallidus external; GPI, globus pallidus internal; STn, subthalamic nucleus; SNc/r, substantia nigra pars compacta/reticulata; VTA, ventral tegmental area; Glu, glutamate; DA, dopamine; GABA, gamma-aminobutyric acid; ACh, acetylcholine. (Online version in colour.)

timing over a time-scale that far exceeds the longest firing period of any individual neuron. The first population clock model was proposed by Mauk and co-workers [7,31,32] in the context of the cerebellum. Such models consist of possible multiple layers of recurrently connected neural networks, i.e. networks of all-to-all coupled neurons that make it possible for a neuron to indirectly feedback onto itself [30]. Depending on the coupling strengths, the recurrent neural networks can self-maintain reproducible dynamic patterns of activity in response to a certain input. Such autonomous and reproducible patterns of neural activity could offer a reliable model for timing. Another advantage of the population clock models is that for weak couplings the network cannot self-maintain reproducible patterns of activity but instead produces input-dependent patterns of activity. Such a model was recently proposed for sensory timing [30]. Similar firing rate models were used by Itskov *et al.* [33] to design a large recurrently connected neural network that produced precise interval timing. By balancing the contribution of the deterministic and stochastic coupling strengths they showed that the first layer of such a population clock model can produce either a reproducible pattern of activity (associated with a timing ‘task’) or desynchronized pattern of activity that cannot keep track of long time-intervals (‘home cage’) [33]. The rate model of Itskov *et al.* [33] was also capable of extracting accurate interval timing information from a second layer with no recurrent excitation and only a global, non-specific recurrent inhibition. The second layer was driven by both the output of the previous layer (through sparse and random connections) and noise [33].

Finally, a quite different solution was offered by Meck and co-workers [4,34] (figure 2a), who proposed the striatal beat frequency (SBF) in which timing is coded by the coincidental activation of neurons, which produces firing beats with periods spanning a much wider range of durations than single neurons [35]. As Matell & Meck [34] suggested, the interval timing could be the product of multiple and complementary mechanisms. They suggested that the same

neuroanatomical structure could use different mechanisms for interval timing.

Here, we showed analytically that in the context of the proposed SBF neural circuitry, time-scale invariance emerges naturally from variability (noise) in models’ parameters. We also showed that time-scale invariance is independent of both the type of the input neuron and the probability distribution or the sources of the noise. We found that the criterion time noise produces a symmetric Gaussian output that obeys scalar property. On the other hand, the frequency noise produces an asymmetric Gaussian-like output with a long tail that also obeys scalar property.

2. The striatal beat frequency model

(a) Neurobiological justification of a striatal beat frequency model

Our paradigm for interval timing is inspired by the SBF model [4,34], which assumes that durations are coded by the coincidental activation of a large number of cortical (input) neurons projecting onto spiny (output) neurons in the striatum that selectively respond to particular reinforced patterns [36–38] (figure 2a).

(i) Neural oscillators

A key assumption of the SBF model is the existence of a set of neural oscillators able to provide the time base for the interval timing network. There is strong experimental evidence that oscillatory activity is a hallmark of neuronal activity in various brain regions, including the olfactory bulb [39–41], thalamus [42,43], hippocampus [44,45] and neocortex [46]. Cortical oscillators in the alpha band (8–12 Hz [47,48]) were previously considered as pacemakers for temporal accumulation [49], as they reset upon occurrence of the to-be-remembered stimuli [50]. In the SBF model, the neural oscillators are loosely associated with the frontal cortex (FC; figure 2a).

(ii) Working and long-term memories

Among the potential areas involved in storing brain's states related to salient features of stimuli in interval timing trials are the hippocampus (see [51] and references therein) and the striatum, which we mimic in our simplified neural circuitry (figure 2a).

(iii) Coincidence detection with spiny neurons

Support for the involvement of the striato-frontal dopaminergic system in timing comes from imaging studies in humans [52–55], lesion studies in humans and rodents [56,57], and drug studies in rodents [58,59] all pointing towards the basal ganglia (BG) as having a central role in interval timing (see also [60] and references therein). Striatal firing patterns are peak-shaped around a trained criterion time, a pattern consistent with substantial striatal involvement in interval timing processes [61]. Lesions of striatum result in deficiencies in both temporal-production and temporal-discrimination procedures [62]. There are also neurophysiological evidences that striatum can engage reinforcement learning to perform pattern comparisons (reviewed by Sutton & Barto [63]). Another reason we ascribed the coincidence detection to medium spiny neurons is due to their bistable property that permits selective filtering of incoming information [64,65]. Each striatal spiny neuron integrates a very large number of afferents (between 10 000 and 30 000) [36,37,65], of which a vast majority ($\approx 72\%$) are cortical [47,66].

(iv) Biological noise and network activity

The activity of any biological neural network is inevitably affected by different sources of noise, e.g. channel gating fluctuations [67,68], noisy synaptic transmission [69] and background network activity [70–72]. Single-cell recordings support the hypothesis that irregular firing in cortical interneurons is determined by the intrinsic stochastic properties (channel noise) of individual neurons [73,74]. At the same time, fluctuations in the presynaptic currents that drive cortical spiking neurons have a significant contribution to the large variability of the interspike intervals [75,76]. For example, in spinal neurons, synaptic noise alone fully accounts for output variability [75]. Additional variability affects either the storage (writing) or retrieval (reading) of criterion time to or from the memory [77,78]. Another source of criterion time variability comes from considerations of how animals are trained [79,80]. In this paper, we were not concerned with the biophysical mechanisms that generated irregular firing of cortical oscillators nor did we investigate how reading/writing errors of criterion time happened. We rather investigated whether the above assumed variabilities in the SBF model's parameters can produce *accurate* and *time-scale invariant* interval timing.

(b) Numerical implementation of a striatal beat frequency model

(i) Neural oscillators

Neurons that produce stable membrane potential oscillations are mathematically described as limit cycle oscillators, i.e. they pose a closed and stable phase space trajectory [81]. Because the oscillations repeat identically, it is often convenient to map the high-dimensional space of periodic oscillators using a phase variable that continuously covers

the interval $(0, 2\pi)$. Phase oscillator models have a series of advantages: (i) they provide analytical insights into the response of complex networks; (ii) any neural oscillator can be reduced to a phase oscillator near a bifurcation point [82]; and (iii) they allow numerical checks in a reasonable time. All neurons operate near a bifurcation, i.e. a point past which the neuron produces large membrane potential excursions—called action potentials [81].

In this SBF-sin implementation, the cortical neurons, presumably localized in the FC (figure 2a), are represented by N_{in} (input) phase oscillators with intrinsic frequencies $f_i (i = 1, \dots, N_{\text{in}})$ uniformly distributed over the interval $(f_{\text{min}}, f_{\text{max}})$, projecting onto N_{out} (output) spiny neurons [34] (figure 2b). A sine wave is the simplest possible phase oscillator that mimics periodic transitions between hyperpolarized and depolarized states observed in single-cell recordings. For analytical purposes, the membrane potential of the i th cortical neuron was approximated by a sine wave $v_i(t) = a \cos(2\pi f_i t)$, where a is the amplitude of oscillations. We also implemented an SBF-ML network in which the input neurons are conductance-based Morris–Lecar (ML) model neurons with two state variables: membrane potential and a slowly varying potassium conductance [83,84] (see electronic supplementary material, section A for detailed model equations).

(ii) Working and long-term memories

The memory of the criterion time T is numerically modelled by the set of state parameters (or weights) w_{ij} that characterize the state of cortical oscillator i during the FI trial j . In our implementation of the noiseless SBF-sin model, the weights $w_{ij} \propto v_i(T_j)$, where T_j is the stored value of the criterion time T in the FI trial j . The state of FC oscillators i at the reinforcement time T_j was implemented as the normalized average over all memorized values T_j of the criterion time: $w_i = \sum_{j=1}^{N_{\text{mem}}} v_i(T_j) / \text{norm}$, where we used $\text{norm} = \max\left(\sum_{j=1}^{N_{\text{mem}}} v_i(T_j)\right) \leq N_{\text{mem}}$ such that the normalized weight is bounded $|w_i| \leq 1$ (figure 2b). We found no difference between the response of the SBF model with the above weights or the positively defined weight $w_i = \sum_{j=1}^{N_{\text{mem}}} (1 + v_i(T_j)) / 2 \text{norm}$.

(iii) Coincidence detection with spiny neurons

The comparison between a stored representation of an event, e.g. the set of the states of cortical oscillators at the reinforcement (criterion) time w_i , and the current state $v_i(t)$ of the same cortical oscillators during the ongoing test trial is believed to be distributed over many areas of the brain [85]. Based on neurobiological data, in our implementation of the striato-cortical interval timing network, we have a ratio of 1000:1 between the input (cortical) oscillators and output (spiny) neurons in the BG (figure 2b). The output neurons, which mimic the spiny neurons in the BG, act as coincidence detectors: they fire when the pattern of activity (or the state of cortical oscillators) $w_i(t)$ at the current time t matches the memorized reference weights w_i . Numerically, the coincidence detection was modelled using the product of the two sets of weights:

$$\text{out}(t) = \sum_{i=1}^{N_{\text{in}}} w_i v_i(t). \quad (2.1)$$

The purpose of the coincidence detection given by equation (2.1) is to implement a rule that produces a strong output

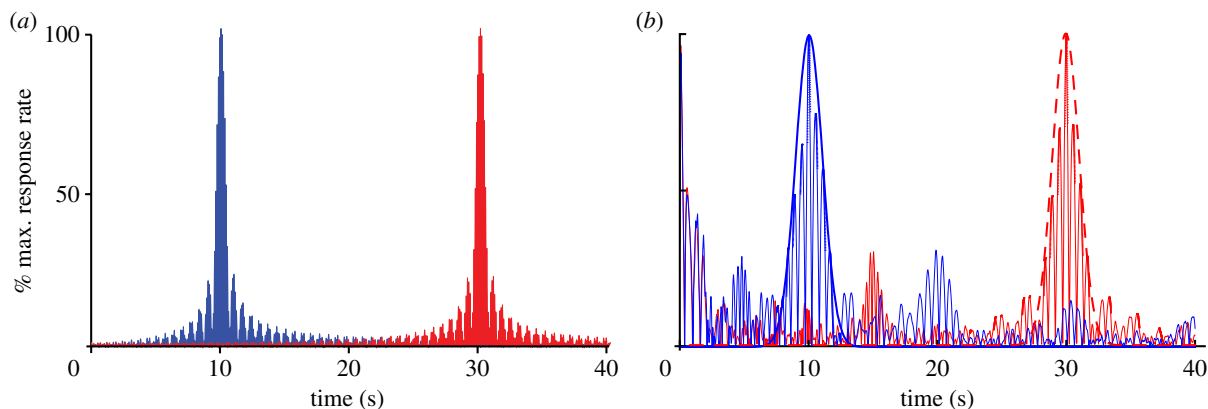


Figure 3. A noise-free SBF model does not produce time-scale invariance. Numerically generated output of a noise-free SBF-sin (a) and SBF-ML (b) model with $N_{\text{in}} = 1000$ for $T = 10$ and $T = 30$ s. As predicted, the width of the output function of any noise-free SBF model is independent of the criterion time. The Gaussian envelopes are also shown with continuous line (for $T = 10$ s) and dashed line (for $T = 30$ s). (Online version in colour.)

when the two vectors w_i and $v_i(t)$ coincide and a weaker response when they are dissimilar. Although there are many choices, such as sigmoidal functions (which involve numerically expensive calculations owing to exponential functions involved), we opted for implementing the simplest possible rule that would fulfil the above requirement, i.e. the dot product of the vectors w_i and $v_i(t)$. Without reducing the generality of our approach, and in agreement with experimental findings [66], for analytical analyses, we considered only one output neuron ($N_{\text{out}} = 1$) in equation (2.1).

(iv) Biological noise and network activity

Two sources of variability (noise) were considered in this SBF implementation. (i) Frequency variability, which was modelled by allowing the intrinsic frequencies f_i to fluctuate according to a specified probability density function pdf_f , e.g. Gaussian, Poisson, etc. Computationally, the noise in the firing frequency of the respective neurons was introduced by varying either the frequency, f_i (in the SBF-sin implementation), or the bias current I_{bias} required to bring the ML neuron to the excitability threshold (in the SBF-ML implementation). (ii) Memory variability was modelled by allowing the criterion time T to be randomly distributed according to a probability density function pdf_T .

3. Results

(a) No time-scale invariance in a noiseless striatal beat frequency model

In the absence of noise (variability) in the SBF-sin model, the output given by equation (2.1) for $N_{\text{out}} = 1$ is (see electronic supplementary material, section B for detailed calculations):

$$\text{out}(t) = \frac{\cos(a_0(t-T)) \sin(b_0(t-T))}{2 \sin(b_0(t-T)/N_{\text{in}})}, \quad (3.1)$$

where $a_0 = \pi(f_{\text{max}} + f_{\text{min}} - df)$, $b_0 = \pi(f_{\text{max}} - f_{\text{min}})$, and oscillators' frequencies were equally spaced over the frequency range $[f_{\text{min}}, f_{\text{max}}]$, i.e. $f_k = f_{\text{min}} + kdf$ with $df = (f_{\text{max}} - f_{\text{min}})/N_{\text{in}}$ and $k = 0, \dots, N_{\text{in}} - 1$. The envelope of the output function is given by the slowly oscillating function $\sin(b_0(t-T))/(2\sin(b_0(t-T)/N_{\text{in}}))$.

The width, σ_{out} , of the output function is determined from the condition that the output function amplitude at $t = T + \sigma_{\text{out}}/2$, i.e. $\text{out}(t = T + \sigma_{\text{out}}/2)$, is half of its maximum possible amplitude, i.e. $1/2_{\text{out}}(t = T)$. Based on equation (3.1), we predicted theoretically that in the absence of noise σ_{out} is independent of the criterion time and violates time-scale invariance (see electronic supplementary material, section B for detailed calculations).

To numerically verify the above predictions, the envelope of the output function of a noise-free SBF-sin model was fitted with a Gaussian whose mean and standard deviations were contrasted against the theoretically predicted values (figure 3a). The width of the envelope is constant regardless of the criterion time and it matches the theoretical prediction.

The above result regarding the emergence of time-scale property from noise in the SBF-sin model can extend to any type of input neuron. Indeed, according to Fourier's theory, any periodic train of action potentials can be decomposed into discrete sine-wave components. It results that irrespective of the type of input neuron, a noise-free SBF model cannot produce time-scale invariant outputs. We verified this prediction by replacing the sine-wave oscillator inputs with biophysically realistic *noise-free* ML neurons (figure 3b). Numerical simulations confirmed that the envelope of the output function of the SBF-ML model can be reasonably fitted by a Gaussian (see [48,86,87]), but the width of the Gaussian output does not increase with the timed interval (figure 3b), thus violating the time-scale invariance (scalar property).

(b) Time-scale invariance emerges from criterion time noise in the striatal beat frequency model

Many sources of noise (variability) may affect the functioning of an interval timing network, such as small fluctuations in the intrinsic frequencies of the inputs, and in the encoding and retrieving the weights $w_i(T)$ by the output neuron(s) [34,35,86–88]. Here, we showed analytically that one noise source is sufficient to produce time-scale invariance [34,48]. Without compromising generality, in the following, we examined the role of the variability in encoding and retrieval of the criterion time by the output neuron(s). The cumulative effect of all noise sources (trial-to-trial variability, neuromodulatory inputs, etc.) on the memorized weights w_i was modelled by

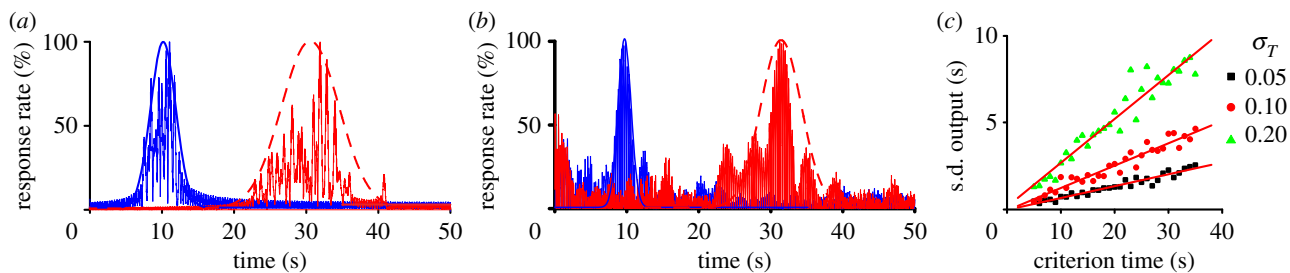


Figure 4. Time-scale invariance emerges from criterion time noise in the SBF model. (a) Time-scale invariance emerges spontaneously in a noisy SBF-sin model; here, the two criteria are $T = 10$ and $T = 30$ s. The output functions (thin continuous lines) were fitted with Gaussian curves (thick continuous line for $T = 10$ s and dashed line for $T = 30$ s) in order to estimate the position of the peak and the width of the output function. In an SBF-sin model, the standard deviation of the output function increases linearly with the criterion time. (b) In an SBF-ML implementation, the output function still has a Gaussian shape (owing to central limit theorem) and its width increases with criterion time. (c) Numerical simulations confirm that the standard deviation of the output function σ_{out} increases linearly with the criterion time T , which is the hallmark of time-scale invariance. Furthermore, for Gaussian memory variance we also found that σ_{out} is proportional to the standard deviation of the noise σ_T . (Online version in colour.)

the stochastic variable T_j distributed around T according to a given pdf_T . For $N_{\text{out}} = 1$, the output function given by equation (2.1) becomes (see electronic supplementary material, section C for detailed calculations):

$$\text{out}(t) = \frac{1}{2} \sum_{i=1}^{N_{\text{in}}} \sum_{j=1}^{N_{\text{trials}}} \cos(2\pi f_i(t - T_j)). \quad (3.2)$$

Based on the central limit theorem, the output function given by equation (3.2), which is a sum of a (very) large number N_{trials} of stochastic variables T_j , is always a Gaussian, regardless of the pdf_T of the criterion time. We used the estimated value of stochastic output function given by equation (3.2) and found that (see electronic supplementary material, section C for detailed calculations): (i) the output function is always Gaussian (based on the central limit theorem), (ii) peaks at $t_{0T} = T(1 + \gamma_T) \approx T$ and (iii) the standard deviation of the output function σ_{out} is proportional to the criterion time T , i.e. obeys the scalar property.

(c) Particular case: infinite frequency range and time-scale invariance in the presence of Gaussian noise affecting the memorized criterion time

Although we already showed that the output function for the SBF-sin model and arbitrary pdf_T for the criterion time noise is always Gaussian, produces accurate interval timing and obeys scalar property, it is illuminating to grasp the meaning of the theoretical coefficients in our general result by investigating a biologically relevant particular case. If the criterion time is affected by a Gaussian noise with zero mean and standard deviation σ_T , then one can show that (see electronic supplementary material, section D for detailed calculations), in the limit of a very large pool (theoretically infinite) of inputs, the output function of the SBF-sin model is

$$\text{out}(t) = \frac{1}{4T\sigma_T\sqrt{2\pi}} e^{-(t-T)^2/2T^2\sigma_T^2}. \quad (3.3)$$

The output function given by equation (3.3) with the physically realizable term centred at $t = T$: (i) has a Gaussian (as predicted by the central limit theorem), (ii) peaks at $t = T$, i.e. produces accurate timing and (iii) has a standard deviation

$$\sigma_{\text{out}} = T\sigma_T, \quad (3.4)$$

which obeys scalar property. We previously showed that for arbitrary noise distributions affecting the criterion time, the

peak of the output function should be at $t_{0T} = T(1 + \gamma_T)$. The actual peak in the presence of the Gaussian noise is at $t = T$, which shows that in this particular case $\gamma_T = 0$.

(d) Particular case: finite frequency range and time-scale invariance in the presence of Gaussian noise affecting the memorized criterion time

In our previous numerical implementations of the SBF model [48,86,87], the frequency range was finite and coincides with α band (8–12 Hz). Is the SBF model still performing accurate and scalar interval timing under such a strong restriction? For a finite range of frequencies ($f_{\text{min}} < f < f_{\text{max}}$) with a very large number of FC oscillators N_{in} , a more realistic estimation of the output function from equation (3.2) is (see electronic supplementary material, section E for detailed calculations):

$$\text{out}(t) \approx \frac{\text{Erf}(\sqrt{2\pi}f_{\text{max}}T\sigma_T) - \text{Erf}(\sqrt{2\pi}f_{\text{min}}T\sigma_T)}{4T\sigma_T\sqrt{2\pi}} e^{-(t-T)^2/2T^2\sigma_T^2}, \quad (3.5)$$

where $\text{Erf}(f)$ is the error function. A major difference between the equation (3.3), which is valid in the limit of an infinite range of frequencies of the FC oscillators, and the equation (3.5), which takes into account the fact that there is always only a finite frequency range of FC oscillators, is the frequency-dependent amplitude of the output function represented by the difference of the two $\text{Erf}(f)$ functions. Therefore, we proved that even for a finite frequency range of the FC oscillators the output function given by equation (3.5) is (i) Gaussian (ii) centred on the criterion time T , and obeys scalar property with a width

$$\sigma_{\text{out}} = T\sigma_T. \quad (3.6)$$

We used the SBF-sin implementation to numerically verify our theoretical prediction that $\sigma_{\text{out}} = T\sigma_T$ over multiple trials (runs) of this type of stochastic process and for different values of T . The output functions (see continuous lines in figure 4a) for $T = 10$ s and $T = 30$ s are reasonably fitted by Gaussian curves. Our numerical results show a linear relationship between σ_{out} of the Gaussian fit of the output and T . We found that the resultant slope of this linear relationship matched the theoretical prediction given by $\sigma_{\text{out}} = T\sigma_T$. For example, for $\sigma_T = 10\%$ the average slope was $11.3\% \pm 4.5\%$ with a coefficient of determination of $R^2 = 0.93$, $p < 10^{-4}$. We also found that for the SBF-ML the width of the Gaussian envelope increases

linearly with the criterion time (figure 4b). For example, figure 4c shows the slope of the standard deviation σ_{out} versus criterion time for different values of the standard deviation of the Gaussian noise. Figure 4c shows not only that the scalar property is valid, but it also shows that $\sigma_{\text{out}} \propto \sigma_T T$ as we predicted theoretically. Indeed, for $\sigma_T = 0.05$ the numerically estimated proportionality constant is 0.068 (filled squares in figure 4c, $R^2 = 0.97$) for $\sigma_T = 0.1$ the slope is 0.129 (filled circles in figure 4c, $R^2 = 0.96$) and for $\sigma_T = 0.2$ the slope is 0.25 (filled triangles in figure 4c, $R^2 = 0.96$).

(e) Time-scale invariance emerges from frequency variance during probe trials in the striatal beat frequency model

In addition to memory variance, frequency fluctuations owing to stochastic channel noise or background networks activity has received considerable attention. Here, we considered only frequency variability during the probe trial and assumed that there was no frequency variability during the FI procedure while the weights w_i were memorized. We also assumed that there is no variability in the memorized criterion time, because its effect on interval timing was already addressed in §3d.

The cumulative effect of all noise sources on the firing frequencies during the probe trials was modelled by the stochastic variable f_{ij} distributed around the frequency f_i according to a given pdf $_f$. Based on equation (2.1) with $N_{\text{out}} = 1$, the output function term centred around $t = T$ becomes (see electronic supplementary material, section F for detailed calculations):

$$\text{out}(t) = \frac{1}{2} \sum_{i=1}^{N_{\text{in}}} \sum_{j=1}^{N_{\text{trials}}} \cos(2\pi(f_{ij}t - f_iT)). \quad (3.7)$$

Based on the central limit theorem, the output function given by equation (3.7), which is the sum of a (very) large number N_{trials} of stochastic variables f_{ij} , is always a Gaussian, regardless of the pdf $_f$. We used the average value of the stochastic equation (3.7) to estimate the output function and found that (see electronic supplementary material, section F for detailed calculations) it is always: (i) Gaussian (based on the central limit theorem), (ii) peaks at $t_{\text{of}} = T/(1 + \gamma_f) \approx T$ and (iii) has a standard deviation σ_{out} that increases linearly with the criterion time T

$$\sigma_{\text{out}} = T(1 + \gamma_T)\sigma_f, \quad (3.8)$$

i.e. obeys scalar property.

(f) Particular case: infinite frequency range and time-scale invariance in the presence of Gaussian noise affecting oscillators' frequencies during probe trials

As in §2e, we used a Gaussian distribution pdf $_f$ to explicitly compute the theoretical coefficients in the above general result. Briefly, by replacing the stochastic frequencies f_{ij} with an appropriate Gaussian distribution $f_i(1 + \text{Gauss}(0, \sigma_f))$, we found that the output function is (see electronic supplementary material, section G for detailed calculations):

$$\text{out}(t) = \frac{e^{-(T/t-1)^2/2\sigma_f^2}}{4\sigma_f t \sqrt{2\pi}}, \quad (3.9)$$

which looks like a Gaussian with a very long tail (figure 5a) and peaks at $t_{\text{of}} = 2T/(1 + \sqrt{1 + 4\sigma_f^2})$. The skewness of the

output function increases with the standard deviation of the frequency noise σ_f . For $t < t_{\text{of}}$, the half-width $\Delta\tau_1$ increases with the standard deviation of the frequency noise σ_f , although at a much slower rate than $\Delta\tau_2$ for $t > t_{\text{of}}$ (figure 5b). This fact is reflected in a faster than linear increase of the $\Delta\tau_2/\Delta\tau_1$ against σ_f (figure 5c). The quadratic fit over the entire $\sigma_f \in [0, 1]$ shown in figure 5c is given by $\Delta\tau_2/\Delta\tau_1 = (0.902 \pm 0.007) + (3.74 \pm 0.03)\sigma_f + (-1.27 \pm 0.03)\sigma_f^2$ with an adjusted $R^2 = 0.999$. For reasonable standard deviation of the frequency noise $\sigma_f < 0.5$, we found that $\Delta\tau_2/\Delta\tau_1 = (0.967 \pm 0.003) + (3.03 \pm 0.01)\sigma_f$ with an adjusted $R^2 = 0.999$. As the output function given by equation (3.9) is no longer symmetric with respect to the peak located at $t_{\text{of}} = 2T/(1 + \sqrt{1 + 4\sigma_f^2})$, the width of the output function is given $\sigma_{\text{out}} = t_{\text{of}}(x_2 - x_1)$, where x_1 and x_2 are the solutions of the half-width equation $\text{out}(x) = 1/2\text{out}(1)$. We found (figure 5d) that the width of the output function $\sigma_{\text{out}} = (-0.025 \pm 0.002) + (2.707 \pm 0.009)\sigma_f + (-0.974 \pm 0.008)\sigma_f^2$ with an adjusted $R^2 = 0.9999$ over the entire range $\sigma_f \in [0, 1]$. A reasonable approximation for standard deviation of the frequency noise $\sigma_f < 0.5$ is linear $\sigma_{\text{out}} = (0.019 \pm 0.003) + (2.20 \pm 0.01)\sigma_f$ with an adjusted $R^2 = 0.999$. As a result, in the presence of frequency variability during probe trials, we predict theoretically that the SBF model (i) produces a Gaussian-like output function with a long tail, (ii) produces accurate interval timing (the output function is centred on $t_{\text{of}} = 2T/(1 + \sqrt{1 + 4\sigma_f^2}) \approx T$) and (iii) obeys scalar property with $\sigma_{\text{out}} \propto T\sigma_f$. We also noted that the peak time predicted for an arbitrary pdf $_f$, i.e. $t_{\text{of}} = T/(1 + \gamma_f)$ is identical with the peak time in the particular case of Gaussian noise, i.e. $t_{\text{of}} = 2T/(1 + \sqrt{1 + 4\sigma_f^2})$ if $\gamma_f = (\sqrt{1 + 4\sigma_f^2} - 1)/2 \approx \sigma_f^2$ for $\sigma_f \ll 1$.

(g) Particular case: finite frequency range and time-scale invariance in the presence of Gaussian noise affecting oscillators' frequencies during probe trials

For a finite range of frequencies ($f_{\text{min}} < f < f_{\text{max}}$) with a very large number of FC oscillators N_{inv} , a more realistic estimation of the output function from equation (3.7) is (see electronic supplementary material, section H for detailed calculations):

$$\text{out}(t) \approx \frac{\text{Erf}(\sqrt{2}\pi f_{\text{max}}\sigma_f t) - \text{Erf}(\sqrt{2}\pi f_{\text{min}}\sigma_f t)}{4\sqrt{2}\pi\sigma_f t} e^{-(t-T)^2/2\sigma_f^2}. \quad (3.10)$$

A significant difference between equation (3.9), which is valid in the limit of an infinite frequency range of the FC oscillators, and equation (3.10), which takes into consideration that there is always only a finite frequency range of the FC oscillators, is the frequency-dependent factor in the output function represented by the difference of the two Erf() functions. The output function in equation (3.10) resembles a Gaussian with a long tail and obeys time-scalar invariance property.

We used both the SBF-sin and SBF-ML implementations to numerically verify that (i) the output function resembles a Gaussian with a long tail (figure 6a), and (ii) the width of the output function increases linearly with the criterion time (figure 6b). The output functions of the SBF-ML implementation (see thin continuous lines in figure 6a) for

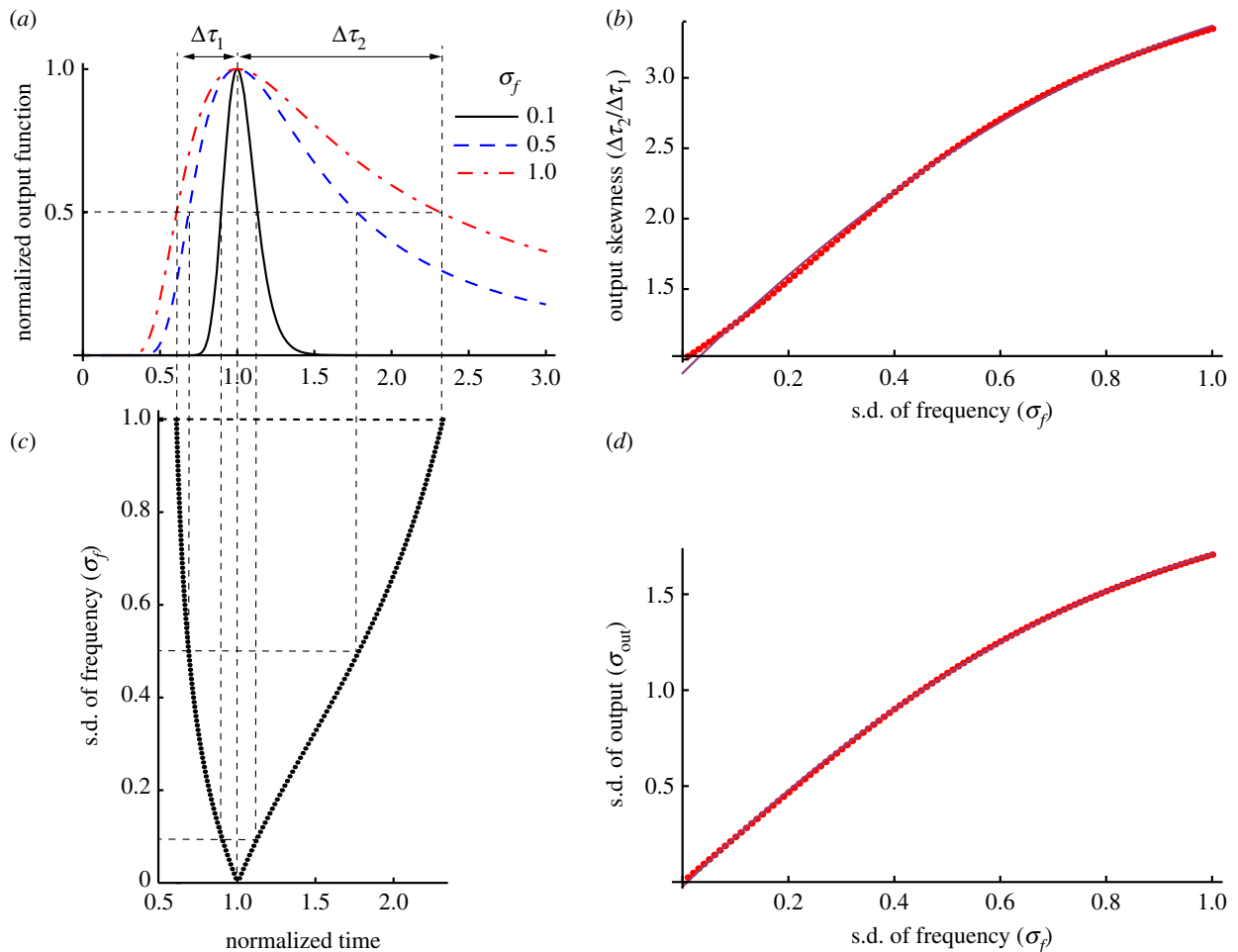


Figure 5. Frequency noise produces a skewed Gaussian-like output with a long tail—theoretical predictions. (a) Theoretically predicted output function for Gaussian noise affecting the oscillators' frequencies is a skewed Gaussian-like output. The normalized output function is plotted against the normalized time t/t_{0f} , where t_{0f} is the time marker for the peak of the output function. The skewness is measured by the two corresponding half-widths τ_1 and τ_2 . (b) Although both half-widths increase with the standard deviation of the frequency noise, the long tail of the output is determined by the very fast increase of τ_2 . (c) A quantitative measure of the skewness is the ratio τ_2/τ_1 , which increases faster than linearly with σ_f . (d) The width of the output function σ_{out} also increases faster than linearly with σ_f . (Online version in colour.)

$T = 10$ s and $T = 30$ s are reasonably fitted by Gaussian curves (see thick continuous line for $T = 10$ s and dashed line for $T = 30$ s in figure 6a). However, as predicted theoretically, the output has a long tail. The scalar property is indeed valid, because the width of the output function linearly increase with the criterion time (figure 6b).

Furthermore, we checked that the scalar property holds not only for Gaussian noise, which allowed us to determine an analytic expression for the long-tailed output function in §4f, but also for uniform and Poisson noise.

4. Discussion

Computational models of interval timing vary largely with respect to the hypothesized mechanisms and the assumptions by which temporal processing is explained, and by which time-scale invariance or drug effects are explained. The putative mechanisms of timing rely on pacemaker/accumulator processes [5,6,89,90], sequences of behaviours [20], pure sine oscillators [8,34,91,92], memory traces [21,93–97] or cell and network-level models [27,98]. For example, both neurometric functions from single neurons and ensembles of neurons successfully paralleled the psychometric functions for the to-be-timed intervals shorter than 1 s [27]. Reutimann *et al.* [99] also considered interacting populations

that are subject to neuronal adaptation and synaptic plasticity based on the general principle of firing rate modulation in a single cell. Balancing long-term potentiation (LTP) and long-term depression (LTD) mechanisms are thought to modulate the firing rate of neural populations with the net effect that the adaptation leads to a linear decay of the firing rate over time. Therefore, the linear relationship between time and the number of clock ticks of the pacemaker–accumulator model in SET [5] was translated into a linearly decaying firing rate model that maps time and variable firing rate.

By and large, to address time-scale invariance, current behavioural theories assume convenient computations, rules or coding schemes. Scalar timing is explained as either deriving from computation of ratios of durations [5,6,100], adaptation of the speed at which perceived time flows [20] or from processes and distributions that conveniently scale up in time [21,91,93,95,96]. Some neurobiological models share computational assumptions with behavioural models and continue to address time-scale invariance by specific computations or embedded linear relationships [101]. Some assume that timing involves neural integrators capable of linearly ramping up their firing rate in time [98], whereas others assume LTP/LTD processes whose balance leads to a linear decay of the firing rate in time [99]. It is unclear whether such models can account for time-scale invariance in a large range of behavioural or neurophysiological manipulations.

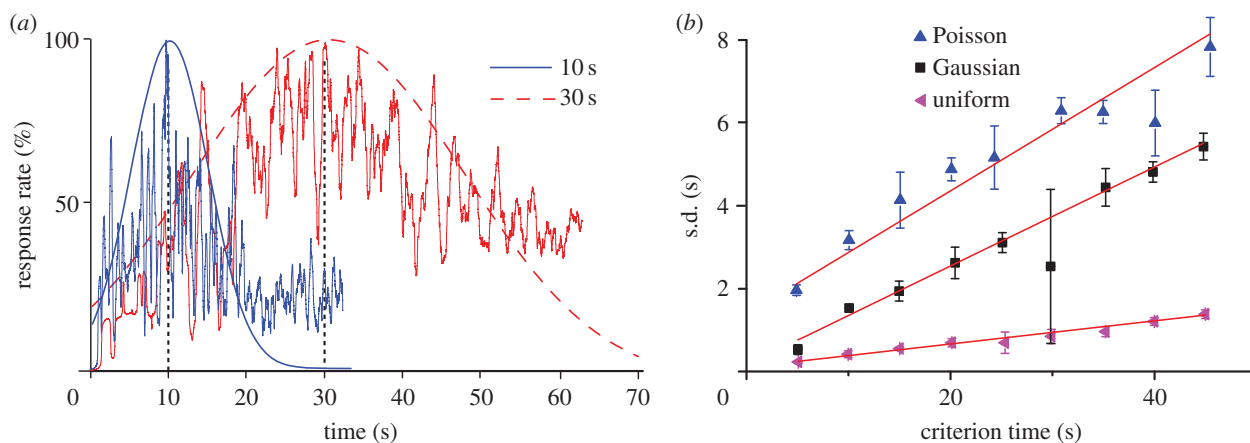


Figure 6. Frequency noise produces a skewed Gaussian-like output with a long tail in numerical results. (a) The output function (thin continuous lines) of the SBF-ML model for $T = 10$ and $T = 30$ s has a Gaussian shape and its peak can be reasonably localized by a Gaussian fit (thick continuous line for $T = 10$ and dashed line for $T = 30$ s). The effect of frequency noise is the asymmetric output function that has a long tail. (b) The width of the output function increases linearly with the criterion time and obey the time-scale invariance property. (Online version in colour.)

Neurons are often viewed as communications channels that respond even to the precisely delivered stimuli sequence in a random manner consistent with Gaussian noise [102]. Biological noise was shown to play important functional roles, e.g. enhance signal detection through stochastic resonance [103,104] and stabilize synchrony [105,106]. Firing rate variability in neural oscillators also results from ongoing cortical activity (see [106,107] and references therein), which may appear noisy simply because it is not synchronized with obvious stimuli.

A possible common ground for all interval timing models could be the threshold accommodation phenomenon that allows stimulus selectivity [108,109] and promotes coincidence detection [11]. Farries [110] showed that dynamic threshold change in subthalamic nucleus (STn) that projects to the output nuclei of the BG allows STn to act either as an integrator for rate code inputs or a coincidence detector [110] (figure 2). Interestingly, under both conditions, faulty (noisy) processing explains time-scale invariance. For example, Killeen & Taylor [28] explained scale invariance of counting in terms of noisy information transfer between counters. Similarly, here, we explained time-scale invariance of timing in terms of noisy coincidence detection during timing. Therefore, it seems that when BG acts either as a counter or as coincidence detector, neural noise alone can explain time-scale invariance.

Our theoretical predictions based on an SBF model show that time-scale invariance emerges as the property of a (very) large and noisy network. Furthermore, we showed that the output function of an SBF mode always resembles the Gaussian shape found in behavioural experiments, regardless of the type of noise affecting the timing network. We showed analytically that in the presence of arbitrary criterion variability alone the SBF model produces an output that (i) has a symmetric and Gaussian shape, (ii) is accurate, i.e. the peak of the output is located at $t_{OT} = T(1 + \gamma_T)$, where $\gamma_T \ll 1$ is a constant that depends on the type of memory noise and (iii) has a width that increases linearly with the criterion time, i.e. obeys time-scale invariance property. The memory variability is ascribed to storing or retrieving the representation of criterion time to and from the long-term memory (figure 2b). We also showed analytically and verified

numerically that for a Gaussian noise affecting the memory of the criterion time the output function of SBF-sin model is analytic and its peak is at $t_{OT} = T$, which means that for Gaussian noise $\gamma_T = 0$ (figure 4a). All of the above properties were also verified by replacing phase oscillators with biophysically realistic ML model neurons (figure 4b,c).

We also showed analytically that, in the presence of arbitrary frequency variability alone, the SBF model produces an output that (i) has a Gaussian-like shape (based on the central limit theorem), (ii) is accurate, i.e. the peak of the output is located at $t_{OT} = T/(1 + \gamma_f)$, where $\gamma_f \ll 1$ is a constant that depends on the type of frequency noise and (iii) has a width $\sigma_{out} = T(1 + \gamma_T)\sigma_f$ that increases linearly with the criterion time, i.e. obeys time-scale invariance property. In the presence of Gaussian noise, the output function is analytic, asymmetric and Gaussian-like (figure 5a) with a skewness that increases quadratically with the standard deviation of the frequency noise (figure 5b). In addition to the fact that the standard deviation of the output function is proportional to the criterion time and, therefore, obeys the time-scale invariance property, it also increases quadratically with the standard deviation of the frequency noise (figure 5d). For Gaussian noise, the peak of the asymmetric, long-tailed Gaussian-like output (figure 5a) resembles experimental data that show a strong long tail in subjects' responses (figure 1c).

Our results regarding the effect of noise on interval timing support and extend the speculation [34] by which an SBF model requires at least one source of variance (noise) to address time-scale invariance. Rather than being a signature of higher-order cognitive processes or specific neural computations related to timing, time-scale invariance naturally emerges in a massively connected brain from the intrinsic noise of neurons and circuits [4,27]. This provides the simplest explanation for the ubiquity of scale invariance of interval timing in a large range of behavioural, lesion and pharmacological manipulations.

Acknowledgements. This work was supported by grants from the National Science Foundation (IOS CAREER award 1054914 to S.A.O.) and the National Institutes of Health (National Institute of Mental Health grants nos. MH065561 and MH073057 to C.V.B.).

References

- Gallistel CR. 1990 *The organization of behavior*. Cambridge, MA: MIT Press.
- Catania AC. 1970 *Reinforcement schedules and psychophysical judgments: a study of some temporal properties of behavior*, pp. 1–42. New York, NY: Appleton-Century-Crofts.
- Roberts S. 1981 Isolation of an internal clock. *J. Exp. Psychol. Anim. Behav. Process.* **7**, 242–268. (doi:10.1037/0097-7403.7.3.242)
- Buhusi CV, Meck WH. 2005 What makes us tick? Functional and neural mechanisms of interval timing. *Nat. Rev. Neurosci.* **6**, 755–765. (doi:10.1038/nrn1764)
- Gibbon J. 1977 Scalar expectancy theory and Weber's law in animal timing. *Psychol. Rev.* **84**, 279–325. (doi:10.1037/0033-295X.84.3.279)
- Gibbon J, Church RM, Meck WH. 1984 Scalar timing in memory. *Ann. N.Y. Acad. Sci.* **423**, 52–77. (doi:10.1111/j.1749-6632.1984.tb23417.x)
- Mauk MD, Buonomano DV. 2004 The neural basis of temporal processing. *Annu. Rev. Neurosci.* **27**, 307–340. (doi:10.1146/annurev.neuro.27.070203.144247)
- Matell MS, King GR, Meck WH. 2004 Differential modulation of clock speed by the administration of intermittent versus continuous cocaine. *Behav. Neurosci.* **118**, 150–156. (doi:10.1037/0735-7044.118.1.150)
- Rakitin BC, Gibbon J, Penney TB, Malapani C, Hinton SC, Meck WH. 1998 Scalar expectancy theory and peak-interval timing in humans. *J. Exp. Psychol. Anim. Behav. Process.* **24**, 15–33. (doi:10.1037/0097-7403.24.1.15)
- Meck WH, Malapani C. 2004 Neuropharmacology of timing and time perception. *Cogn. Brain Res.* **21**, 133–137. (doi:10.1016/j.cogbrainres.2004.07.010)
- Buhusi CV, Aziz D, Winslow D, Carter RE, Swearingen JE, Buhusi MC. 2009 Interval timing accuracy and scalar timing in c57bl/6 mice. *Behav. Neurosci.* **123**, 1102–1113. (doi:10.1037/a0017106)
- Meck WH, Church RM, Wenk GL, Olton DS. 1987 Nucleus basalis magnocellularis and medial septal area lesions differentially impair temporal memory. *J. Neurosci.* **7**, 3505–3511.
- Buhusi CV, Meck WH. 2002 Differential effects of methamphetamine and haloperidol on the control of an internal clock. *Behav. Neurosci.* **116**, 291–297. (doi:10.1037/0735-7044.116.2.291)
- Buhusi CV, Meck WH. 2010 *Timing behavior*, vol. 2, pp. 1319–1323. Berlin, Germany: Springer.
- Treisman M. 1963 Temporal discrimination and the indifference interval. Implications for a model of the 'internal clock'. *Psychol. Monogr.* **77**, 1–31. (doi:10.1037/h0093864)
- Church RM, Meck WH, Gibbon J. 1994 Application of scalar timing theory to individual trials. *J. Exp. Psychol. Anim. Behav. Process.* **20**, 135–155. (doi:10.1037/0097-7403.20.2.135)
- Gibbon J. 1992 Ubiquity of scalar timing with Poisson clock. *J. Math. Psychol.* **36**, 283–293. (doi:10.1016/0022-2496(92)90041-5)
- Gallistel CR. 1991 Representations in animal cognition: an introduction. *Cognition* **37**, 1–22. (doi:10.1016/0010-0277(90)90016-D)
- Killeen PR. 1991 *Behaviors time*, vol. 27, pp. 294–334. New York, NY: Academic Press.
- Killeen PR, Fetterman JG. 1988 A behavioral theory of timing. *Psychol. Rev.* **95**, 274–295. (doi:10.1037/0033-295X.95.2.274)
- Staddon JER, Higa JJ. 1999 Time and memory: towards a pacemaker-free theory of interval timing. *J. Exp. Anal. Behav.* **71**, 215–251. (doi:10.1901/jeab.1999.71-215)
- Sendiña Nadal I, Leyva I, Buldú JM, Almendral JA, Boccaletti S. 2009 Entraining the topology and the dynamics of a network of phase oscillators. *Phys. Rev. E* **79**, 046105. (doi:10.1103/PhysRevE.79.046105)
- Talathi SS, Abarbanel HDI, Ditto WL. 2008 Temporal spike pattern learning. *Phys. Rev. E* **78**, 031918. (doi:10.1103/PhysRevE.78.031918)
- Buonomano DV, Merzenich MM. 1995 Temporal information transformed into a spatial code by a neural network with realistic properties. *Science* **267**, 1028–1030. (doi:10.1126/science.7863330)
- Komura Y, Tamura R, Uwano T, Nishijo H, Kaga K, Ono T. 2001 Retrospective and prospective coding for predicted reward in the sensory thalamus. *Nature* **412**, 546–549. (doi:10.1038/35087595)
- Durstewitz D. 2003 Self-organizing neural integrator predicts interval times through climbing activity. *J. Neurosci.* **23**, 5342–5353.
- Leon MI, Shadlen MN. 2003 Representation of time by neurons in the posterior parietal cortex of the macaque. *Neuron* **38**, 317–327. (doi:10.1016/S0896-6273(03)00185-5)
- Killeen PR, Taylor TJ. 2000 How the propagation of error through stochastic counters affects time discrimination and other psychophysical judgments. *Psychol. Rev.* **107**, 430–459. (doi:10.1037/0033-295X.107.3.430)
- Buonomano D, Karmarkar U. 2002 How do we tell time? *Neuroscientist* **8**, 42–51. (doi:10.1177/107385840200800109)
- Buonomano DV, Laje R. 2010 Population clocks: motor timing with neural dynamics. *Trends Cogn. Sci.* **14**, 520–527. (doi:10.1016/j.tics.2010.09.002)
- Buonomano D, Mauk M. 1995 Neural network model of the cerebellum: temporal discrimination and the timing of motor responses. *Neural Comput.* **6**, 38–55. (doi:10.1162/neco.1994.6.1.38)
- Mauk M, Donegan N. 1977 A model of Pavlovian eyelid conditioning based on the synaptic organization of the cerebellum. *Learn. Mem.* **4**, 130–158. (doi:10.1101/lm.4.1.130)
- Itskov V, Curto C, Pastalkova E, Buzsáki G. 2011 Cell assembly sequences arising from spike threshold adaptation keep track of time in the hippocampus. *J. Neurosci.* **31**, 2828–2834. (doi:10.1523/JNEUROSCI.3773-10.2011)
- Matell MS, Meck WH. 2004 Cortico-striatal circuits and interval timing: coincidence detection of oscillatory processes. *Cogn. Brain Res.* **21**, 139–170. (doi:10.1016/j.cogbrainres.2004.06.012)
- Miall RC. 1989 The storage of time intervals using oscillating neurons. *Neural Comput.* **1**, 359–371. (doi:10.1162/neco.1989.1.3.359)
- Beiser DG, Houk JC. 1998 Model of cortical-basal ganglionic processing: encoding the serial order of sensory events. *Clin. Neurophysiol.* **79**, 3168–3188.
- Houk JC. 1995 *Information processing in modular circuits linking basal ganglia and cerebral cortex*, pp. 3–10. Cambridge, MA: MIT Press.
- Houk JC, Davis JL, Beiser DG. 1995 *Computational neuroscience, models of information processing in the basal ganglia*. Cambridge, MA: MIT Press.
- Beshel J, Kopell N, Kay LM. 2007 Olfactory bulb gamma oscillations are enhanced with task demands. *J. Neurosci.* **27**, 8358–8365. (doi:10.1523/JNEUROSCI.1199-07.2007)
- Kay LM, Lazzara P. 2010 How global are olfactory bulb oscillations? *J. Neurophysiol.* **104**, 1768–1773. (doi:10.1152/jn.00478.2010)
- Martin C, Houitte D, Guillemier M, Petit F, Bonvento G, Gurden H. 2012 Alteration of sensory-evoked metabolic and oscillatory activities in the olfactory bulb of GLAST-deficient mice. *Front. Neural Circ.* **6**, 1–12. (doi:10.3389/fncir.2012.00001)
- Hughes SW, Lorincz ML, Parri HR, Crunelli V. 2011 Infraslow (<0.1 Hz) oscillations in thalamic relay nuclei basic mechanisms and significance to health and disease states. *Prog. Brain Res.* **193**, 145–162.
- Steriade M, Jones EG, Llinas RR. 1990 *Thalamic oscillations and signaling*. Oxford, UK: John Wiley and Sons.
- Buzsáki G. 2002 Theta oscillations in the hippocampus. *Neuron* **33**, 325–340. (doi:10.1016/S0896-6273(02)00586-X)
- Pignatelli M, Beyeler A, Leinekugel X. 2012 Neural circuits underlying the generation of theta oscillations. *J. Physiol. Paris* **106**, 81–92. (doi:10.1016/j.jphysparis.2011.09.007)
- Worrell GA, Parish L, Cranstoun SD, Jonas R, Baltuch G, Litt B. 2004 High frequency oscillations and seizure generation in neocortical epilepsy. *Brain* **127**, 1496–1506. (doi:10.1093/brain/awh149)
- Brunner F, Kacelnik A, Gibbon J. 1992 Optimal foraging and timing processes in the starling *Sturnus vulgaris*: effect of intercapture interval. *Anim. Behav.* **44**, 597–613. (doi:10.1016/S0003-3472(05)80289-1)
- Buhusi CV, Oprisan SA. 2013 Time-scale invariance as an emergent property in a perceptron with realistic, noisy neurons. *Behav. Process.* **95**, 60–70. (doi:10.1016/j.beproc.2013.02.015)
- Anliker J. 1963 Variations in alpha voltage of the electroencephalogram and time perception. *Science* **140**, 1307–1309. (doi:10.1126/science.140.3573.1307)
- Rizzuto DS, Madsen JR, Bromfield EB, Schulze-Bonhage A, Seelig D, Aschenbrenner-Scheibe R, Kahana MJ. 2003 Reset of human neocortical

- oscillations during a working memory task. *Proc. Natl Acad. Sci. USA* **100**, 7931–7936. (doi:10.1073/pnas.0732061100)
51. Lisman JE, Grace AA. 2005 The hippocampal-VTA loop: controlling the entry of information into long-term memory. *Neuron* **46**, 703–713. (doi:10.1016/j.neuron.2005.05.002)
 52. Coull JT, Vidal F, Nazarian B, Macfar F. 2004 Functional anatomy of the attentional modulation of time estimation. *Science* **303**, 1506–1508. (doi:10.1126/science.1091573)
 53. Harrington DL, Haaland KY. 1999 Neural underpinnings of temporal processing: a review of focal lesion, pharmacological, and functional imaging research. *Rev. Neurosci.* **10**, 91–116. (doi:10.1515/REVNEURO.1999.10.2.91)
 54. Hinton SC, Meck WH, MacFall JR. 1996 Peak-interval timing in humans activates frontal–striatal loops. *Neuroimage* **3**, S224. (doi:10.1016/S1053-8119(96)80226-6)
 55. Stevens MC, Kiehl KA. 2007 Functional neural circuits for mental timekeeping. *Hum. Brain Mapp.* **28**, 394–408. (doi:10.1002/hbm.20285)
 56. Malapani C, Rakitin B, Levy R, Meck WH, Deweer B, Dubois B, Gibbon J. 1998 Coupled temporal memories in Parkinson's disease: a dopamine-related dysfunction. *J. Cogn. Neurosci.* **10**, 316–331. (doi:10.1162/089892998562762)
 57. Meck WH. 1983 Selective adjustment of the speed of internal clock and memory processes. *J. Exp. Psychol. Anim. Behav. Process.* **9**, 171–201. (doi:10.1037/0097-7403.9.2.171)
 58. Meck WH. 1996 Neuropharmacology of timing and time perception. *Cogn. Brain Res.* **3**, 227–242. (doi:10.1016/0926-6410(96)00009-2)
 59. Neil DB, Herndon Jr JG. 1978 Anatomical specificity within rat striatum for the dopaminergic modulation of DRL responding and activity. *Brain Res.* **153**, 529–538. (doi:10.1016/0006-8993(78)90337-2)
 60. Laphis CC, Kroener S, Durstewitz D, Lavin A, Seamans JK. 2007 The ability of the mesocortical dopamine system to operate in distinct temporal modes. *Psychopharmacology (Berl.)* **191**, 609–625. (doi:10.1007/s00213-006-0527-8)
 61. Matell MS, Meck WH, Nicolelis MA. 2003 Interval timing and the encoding of signal duration by ensembles of cortical and striatal neurons. *Behav. Neurosci.* **117**, 760–773. (doi:10.1037/0735-7044.117.4.760)
 62. Jin X, Costa RM. 2010 Start/stop signals emerge in nigrostriatal circuits during sequence learning. *Nature* **466**, 457–462. (doi:10.1038/nature09263)
 63. Sutton RS, Barto AG. 1998 *Reinforcement learning: an introduction*. Cambridge, MA: MIT Press.
 64. Stern EA, Jaeger D, Wilson CJ. 1998 Membrane potential synchrony of simultaneously recorded striatal spiny neurons in vivo. *Nature* **394**, 475–478. (doi:10.1038/28848)
 65. Wilson CJ. 1995 *The contribution of cortical neurons to the firing pattern of striatal spiny neurons*, pp. 29–50. Cambridge, MA: MIT Press.
 66. Doig NM, Moss J, Bolam JP. 2010 Cortical and thalamic innervation of direct and indirect pathway medium-sized spiny neurons in mouse striatum. *J. Neurosci.* **30**, 14 610–14 618. (doi:10.1523/JNEUROSCI.1623-10.2010)
 67. Fellous JM, Tiesinga PHE, Thomas PJ, Sejnowski TJ. 2004 Discovering spike patterns in neuronal responses. *J. Neurosci.* **24**, 2989–3001. (doi:10.1523/JNEUROSCI.4649-03.2004)
 68. White JA, Rubinstein JT, Kay AR. 2000 Channel noise in neurons. *Trends Neurosci.* **23**, 99–115.
 69. Faisal AA, Selen LP, Wolpert DM. 2008 Noise in the nervous system. *Nat. Rev. Neurosci.* **9**, 292–303. (doi:10.1038/nrn2258)
 70. Destexhe A, Rudolph M, Pare D. 2003 The high-conductance state of neocortical neurons in vivo. *Nat. Rev. Neurosci.* **4**, 739–751. (doi:10.1038/nrn1198)
 71. Matsumura M, Cope T, Fetz EE. 1988 Sustained excitatory synaptic input to motor cortex neurons in awake animals revealed by intracellular recording of membrane potentials. *Exp. Brain Res.* **70**, 463–469. (doi:10.1007/BF00247594)
 72. Steriade M, Timofeev I, Grenier F. 2001 Natural waking and sleep states: a view from inside neocortical neurons. *J. Neurophysiol.* **85**, 1969–1985.
 73. Englitz B, Stiefel KM, Sejnowski TJ. 2008 Irregular firing of isolated cortical interneurons in vitro driven by intrinsic stochastic mechanisms. *Neural Comput.* **20**, 44–64. (doi:10.1162/neco.2008.20.1.44)
 74. Markram H, Toledo-Rodriguez M, Wang Y, Gupta A, Silberberg G, Wu C. 2004 Interneurons of the neocortical inhibitory system. *Nat. Rev. Neurosci.* **5**, 793–807. (doi:10.1038/nrn1519)
 75. Calvin WH, Stevens CF. 1968 Synaptic noise and other sources of randomness in motoneuron interspike intervals. *J. Neurophysiol.* **31**, 574–587.
 76. Stevens CF, Zado AM. 1998 Input synchrony and the irregular firing of cortical neurons. *Nat. Neurosci.* **1**, 210–217. (doi:10.1038/659)
 77. Droit-Volet S, Wearden J, Delgado-Yonger M. 2007 Short-term memory for time in children and adults: a behavioral study and a model. *J. Exp. Child Psychol.* **97**, 246–264. (doi:10.1016/j.jecp.2007.02.003)
 78. Fortin C, Couture E. 2002 Short-term memory and time estimation: beyond the 2-second 'critical' value. *Can. J. Exp. Psychol.* **56**, 120–127. (doi:10.1037/h0087390)
 79. Jones LA, Wearden JH. 2003 More is not necessarily better: examining the nature of the temporal reference memory component in timing. *Q. J. Exp. Psychol.* **56**, 321–343. (doi:10.1080/02724990244000287)
 80. Jones LA, Wearden JH. 2004 Double standards: memory loading in temporal reference memory. *Q. J. Exp. Psychol. B* **57**, 55–77.
 81. Izhikevich EM. 2007 *Dynamical systems in neuroscience: the geometry of excitability and bursting*. Cambridge, MA: The MIT Press.
 82. Ermentrout GB. 1986 *Losing amplitude and saving phase*, vol. 66. Berlin, NY: Springer.
 83. Morris C, Lecar H. 1981 Voltage oscillations in the barnacle giant muscle fiber. *Biophys. J.* **35**, 193–213. (doi:10.1016/S0006-3495(81)84782-0)
 84. Rinzel J, Ermentrout B. 1998 *Analysis of neural excitability and oscillations*. Cambridge, MA: MIT Press.
 85. Squire LR, Stark CE, Clark RE. 2004 The medial temporal lobe. *Annu. Rev. Neurosci.* **27**, 279–306. (doi:10.1146/annurev.neuro.27.070203.144130)
 86. Oprisan S, Buhusi C. 2013 How noise contributes to time-scale invariance of interval timing. *Phys. Rev. E* **87**, 052717. (doi:10.1103/PhysRevE.87.052717)
 87. Oprisan SA, Buhusi CV. 2011 Modeling pharmacological clock and memory patterns of interval timing in a striatal beat-frequency model with realistic, noisy neurons. *Front. Integr. Neurosci.* **5**, 52. (doi:10.3389/fnint.2011.00052)
 88. Sobie C, Babul A, de Sousa R. 2011 Neuron dynamics in the presence of 1/f noise. *Phys. Rev. E* **83**, 051912. (doi:10.1103/PhysRevE.83.051912)
 89. Gibbon J, Allan L. 1984 Time perception: introduction. *Ann. N.Y. Acad. Sci.* **423**, 1. (doi:10.1111/j.1749-6632.1984.tb23412.x)
 90. Gibbon J, Church RM. 1984 *Sources of variance in an information processing theory of timing*, pp. 465–488. Hillsdale, NJ: Erlbaum.
 91. Church RM, Broadbent HA. 1990 Alternative representations of time, number, and rate. *Cognition* **37**, 55–81. (doi:10.1016/0010-0277(90)90018-F)
 92. Matell MS, Meck WH. 2000 Neuropsychological mechanisms of interval timing behavior. *Bioessays* **22**, 94–103. (doi:10.1002/(SICI)1521-1878(200001)22:1<94::AID-BIES14>3.0.CO;2-E)
 93. Buhusi CV, Schmajuk NA. 1999 Timing in simple conditioning and occasion setting: a neural network approach. *Behav. Process.* **45**, 33–57. (doi:10.1016/S0376-6357(99)00008-X)
 94. Grossberg S, Merrill JW. 1992 A neural network model of adaptively timed reinforcement learning and hippocampal dynamics. *Brain Res. Cogn. Brain Res.* **1**, 3–38. (doi:10.1016/0926-6410(92)90003-A)
 95. Grossberg S, Schmajuk N. 1989 Neural dynamics of adaptive timing and temporal discrimination during associative learning. *Neural Netw.* **2**, 79–102. (doi:10.1016/0893-6080(89)90026-9)
 96. Machado A. 1997 Learning the temporal dynamics of behavior. *Psychol. Rev.* **104**, 241–265. (doi:10.1037/0033-295X.104.2.241)
 97. Staddon JER, Higa JJ, Chelaru IM. 1999 Time, trace, memory. *J. Exp. Anal. Behav.* **71**, 293–301. (doi:10.1901/jeab.1999.71-293)
 98. Simen P, Balci F, de Souza L, Cohen JD, Holmes P. 2011 A model of interval timing by neural integration. *J. Neurosci.* **31**, 9238–9253. (doi:10.1523/JNEUROSCI.3121-10.2011)
 99. Reutimann J, Yakovlev V, Fusi S, Senn W. 2004 Climbing neuronal activity as an event-based cortical representation of time. *J. Neurosci.* **24**, 3295–3303. (doi:10.1523/JNEUROSCI.4098-03.2004)
 100. Gallistel CR, Gibbon J. 2000 Time, rate, and conditioning. *Psychol. Rev.* **107**, 289–344. (doi:10.1037/0033-295X.107.2.289)

101. Karmarkar UR, Buonomano DV. 2007 Timing in the absence of clocks: encoding time in neural network states. *Neuron* **53**, 427–438. (doi:10.1016/j.neuron.2007.01.006)
102. Borst A, Theunissen FE. 1999 Information theory and neural coding. *Nat. Neurosci.* **2**, 947–957. (doi:10.1038/14731)
103. Benayoun M, Cowan JD, van Drongelen W, Wallace E. 2010 Avalanches in a stochastic model of spiking neurons. *PLoS Comput. Biol.* **6**, e1000846. (doi:10.1371/journal.pcbi.1000846)
104. Gong P-L, Xu J-X. 2001 Global dynamics and stochastic resonance of the forced Fitzhugh–Nagumo neuron model. *Phys. Rev. E* **63**, 031906. (doi:10.1103/PhysRevE.63.031906)
105. Braun HA, Wissing H, Schafer K, Hirsch MC. 1994 Oscillation and noise determine signal transduction in shark multimodal sensory cells. *Nature* **367**, 270–273. (doi:10.1038/367270a0)
106. Kaluza P, Strege C, Meyer-Ortmanns H. 2010 Noise as control parameter in networks of excitable media: role of the network topology. *Phys. Rev. E* **82**, 036104. (doi:10.1103/PhysRevE.82.036104)
107. Kenet T, Bibitchkov D, Tsodyks M, Grinvald A, Arieli A. 2003 Spontaneously emerging cortical representations of visual attributes. *Nature* **425**, 954–956. (doi:10.1038/nature02078)
108. Abarbanel HDI, Talathi SS. 2006 Neural circuitry for recognizing interspike interval sequences. *Phys. Rev. Lett.* **96**, 148104. (doi:10.1103/PhysRevLett.96.148104)
109. Wilentz WB, Contreras D. 2005 Dynamics of excitation and inhibition underlying stimulus selectivity in rat somatosensory cortex. *Nat. Neurosci.* **8**, 1364–1370. (doi:10.1038/nn1545)
110. Farries MA, Kita H, Wilson CJ. 2010 Dynamic spike threshold and zero membrane slope conductance shape the response of subthalamic neurons to cortical input. *J. Neurosci.* **30**, 13 180–13 191. (doi:10.1523/JNEUROSCI.1909-10.2010)